Correlation of oxygen non-stoichiometry to the instabilities and electrochemical performance of $LiNi_{0.8}Co_{0.1}Mn_{0.1}O_2$ utilized in lithium ion battery

Yujing Bi, Wenchao Yang, Rui Du, Jingjing Zhou, Meng Liu, Yang Liu, Deyu Wang*

Ningbo Institute of Materials Technology and Engineering, Chinese Academy of Sciences, Ningbo 315201, China

- Ni/Li disorder is dependent on oxygen deficiency.
- Surface decomposition is related to oxygen defects and storing atmosphere.
- $LiNi_{0.8}Co_{0.1}Mn_{0.1}O_2$ with the least defects presents the best performance.

A B S T R A C T

In this work, we investigate the influence of oxygen non-stoichiometry on the characteristics of $LiNi_{0.8}Co_{0.1}Mn_{0.1}O_2$ cathode material. Among the investigated samples, the level of Ni/Li disorder in the bulk and the thickness of auto-generated layer on the surface share the same trend as the amount of oxygen loss in $LiNi_{0.8}Co_{0.1}Mn_{0.1}O_2$ materials. It indicates that the aforementioned key structural instabilities should be tightly related to the oxygen defects and the induced structural relaxation. As a consequence of structural entirety, the sample with the least defects presents the highest discharge capacity (192.9 $mAhg^{-1}$ at 0.1C), the best rate capability (160.1 $mAhg^{-1}$ at 5C), and the most stable cyclibility (89.9% at 200th). Our results demonstrate that oxygen deficiency plays a key role to determine the electrochemical performance of high-nickel cathode materials.

Keywords:
Oxygen non-stoichiometry
Ni/Li disorder
Surface sensitivity
High nickel cathode
Lithium ion battery

1. Introduction

Inspired by the strong demands on portable electronics, transportation and grids, cathodes with good performance were strongly pursued by academic community and industry. Since firstly proposed in 2000, $LiCo_{1-x-y}Ni_xMn_yO_2$ ($0 < x + y < 1$) cathode materials have rapidly penetrated into the markets of commercial electronics and EV/HEV due to its excellent balance among performance, cost and safety. [1–4] For these cathodes could be considered as the solid solution of $LiCoO_2$, $LiNiO_2$ and $LiMnO_2$ [5,6], the all-round performance of $LiCo_{1-2x}Ni_xMn_xO_2$ is adjustable in some extent as varying the ratio of transitional metal elements. [2,7] Generally speaking, the enhancement of nickel content will improve its discharge capacity, high cobalt stuffs present better rate capability and the samples with more manganese exhibit lower thermal activity. [8–11].

Recently, to meet the ever-increasing demands on high energy density, high-nickel cathode have regained the enormous attentions due to its advantages on reversible capacity and technological maturity when compared with commercial cathodes and Li-rich materials. [12–14] With 4.3 V *vs.* Li/Li^+ as the cut-off potential, these materials could attain a discharge capacity as high as 180–190 $mAhg^{-1}$, [15,16] which is almost 50% higher than that of $LiCoO_2$. However, in most cases, the practical performance was much poorer than the aforementioned value as a result of various barriers, especially attributed to Ni/Li disorder and surface sensitivity.

Ni/Li disorder could deteriorate material's electrochemical property due to the blockage of Li^+ ions transportation passages. [2,12,17–19] The probable reason is widely accepted as the similar ionic radii of Li^+ (0.74 Å) and Ni^{2+} (0.69 Å). However, this hypothesis is challenged by the excellent performance of $LiCo_{1/3}Ni_{1/}$

* Corresponding author.
E-mail address: wangdy@nimte.ac.cn (D. Wang).

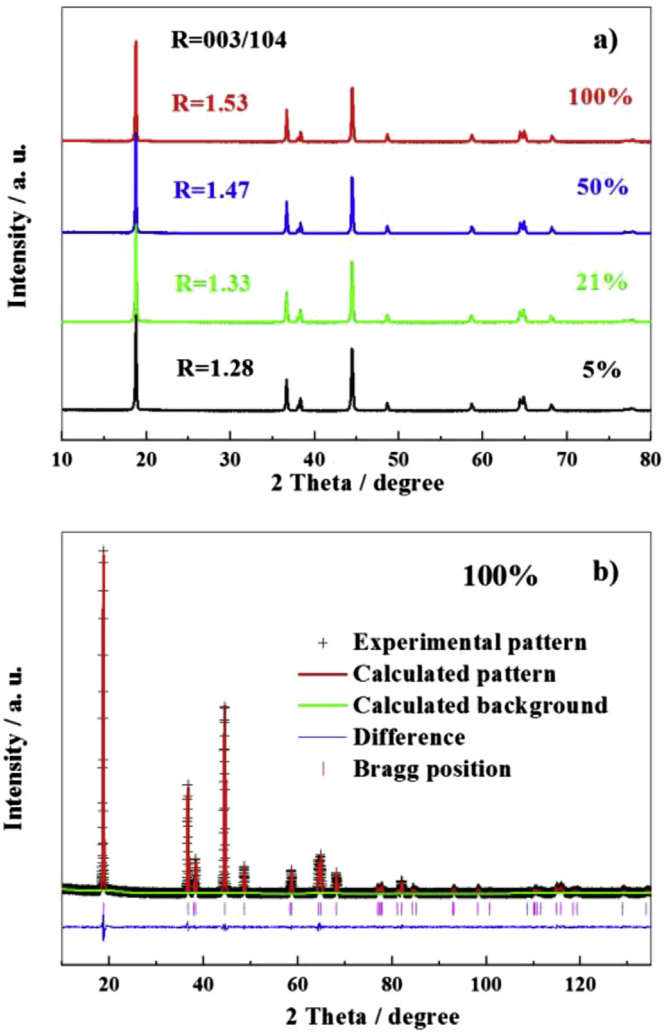

Fig. 1. a) XRD patterns of as-prepared $LiNi_{0.8}Co_{0.1}Mn_{0.1}O_2$ samples; b) refinement pattern of pure O_2 synthesized sample.

$_3Mn_{1/3}O_2$ and $LiCo_{0.2}Ni_{0.4}Mn_{0.4}O_2$ where all nickel ions are 2+. [3,13,20] It seems that Ni/Li disorder should not be the direct results of ionic radii adjacency between Li^+ and Ni^{2+}. As for surface sensitivity, it has been roughly attributed to the strong catalytic capability of nickel, and further explanation was not proposed.

To explore the inherent reasons for these instabilities, we noticed that Ni (III) oxides could lose oxygen more easily than Co(III) oxides and Mn(IV) oxides due to its lower bond energy. [21–23] It means high-Ni cathodes possess much higher possibility to contain oxygen deficiency than $LiCoO_2$ and $LiNi_{1/3}Co_{1/3}Mn_{1/3}O_2$. As a matter of fact, oxygen defects are the most typical structural characteristics and play an evil or positive role on functional ceramics. For example, oxygen defect lowers the thermal sensitivity of $BaTiO_3$ [24] and enables the unique performances of some oxide catalysts and YBCO. [25,26] The performance of high-nickel oxide cathodes should be significantly influenced by this structural variation, which is not thoroughly discussed in our best knowledge.

To clarify this hypothesis, $LiNi_{0.8}Co_{0.1}Mn_{0.1}O_2$ samples are synthesized under various O_2 partial pressures and their characteristics are investigated in this work. According to the results of refinement and thermo-gravimetry, the amount of oxygen non-stoichiometry is monotonically diminished as the increase of oxygen partial pressure. The extent of Ni/Li disorder and the thickness of surface layer share the same variation tendency as that of oxygen defects. Also the probable pathway of surface reaction is modified according to our approaches. The sample with the best structural entirety presents the best electrochemical performance.

Table 1
Crystallographic parameters of the prepared $LiNi_{0.8}Co_{0.1}Mn_{0.1}O_2$ samples.

Oxygen ratio	100%	50%	21%	5%
a/Å	2.8750	2.8754	2.8758	2.8747
c/Å	14.2240	14.2191	14.2144	14.2042
c/a	4.948	4.947	4.943	4.941
V/Å^3	101.826	101.812	101.805	101.650
Ni/Li (3a)	2.85%	3.34%	5.41%	10.97%
6c O occ	0.9748	0.9530	0.9339	0.9185
6c U_{iso}/Å^2	0.0147	0.0112	0.0106	0.0093
Rwp/%	1.11	1.03	0.98	1.06
Rp/%	0.69	0.61	0.63	0.61
CHI^2	2.816	2.807	2.104	3.91

2. Experiment

2.1. Synthesis

$Ni_{0.8}Co_{0.1}Mn_{0.1}(OH)_2$ precursors were synthesized by the co-precipitation method. $Ni(CH_3COO)_2{\cdot}4H_2O$, $Mn(CH_3COO)_2{\cdot}4H_2O$ and $Co(CH_3COO)_2{\cdot}4H_2O$ were dissolved in di-ionic water at 8:1:1 ratio in mole. 1 M LiOH and 0.5 M $NH_3{\cdot}H_2O$ was pumped into the continuous stirring reactor with Ni—Co—Mn aqueous solution to prepare $Ni_{0.8}Co_{0.1}Mn_{0.1}(OH)_2$ precursors. All chemicals were purchased from Aldrich with 99% purity.

$LiNi_{0.8}Co_{0.1}Mn_{0.1}O_2$ samples were prepared with high-temperature solid-state method. The prepared $Ni_{0.8}Co_{0.1}Mn_{0.1}(OH)_2$ was mixed with $LiOH{\cdot}H_2O$ at a molar ratio of 1:1.05 and sintered at 850 °C for 20 h under the atmospheres of pure oxygen, and O_2/N_2 (50: 50, 21: 79, 5:95, v/v) at the same time in the same model ovens. After automatically cooled to room temperature, the samples were stored in the same desiccator for investigation. To diminish the influence of humidity and CO_2 during storage, all the physical characterizations and electrochemical tests were carried out within 24 h after the samples prepared.

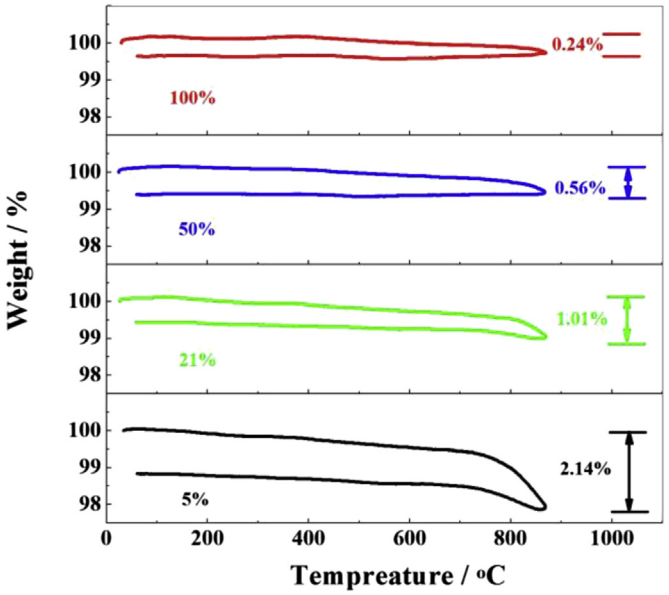

Fig. 2. TG curves at different atmosphere for $LiNi_{0.8}Co_{0.1}Mn_{0.1}O_2$ sample.

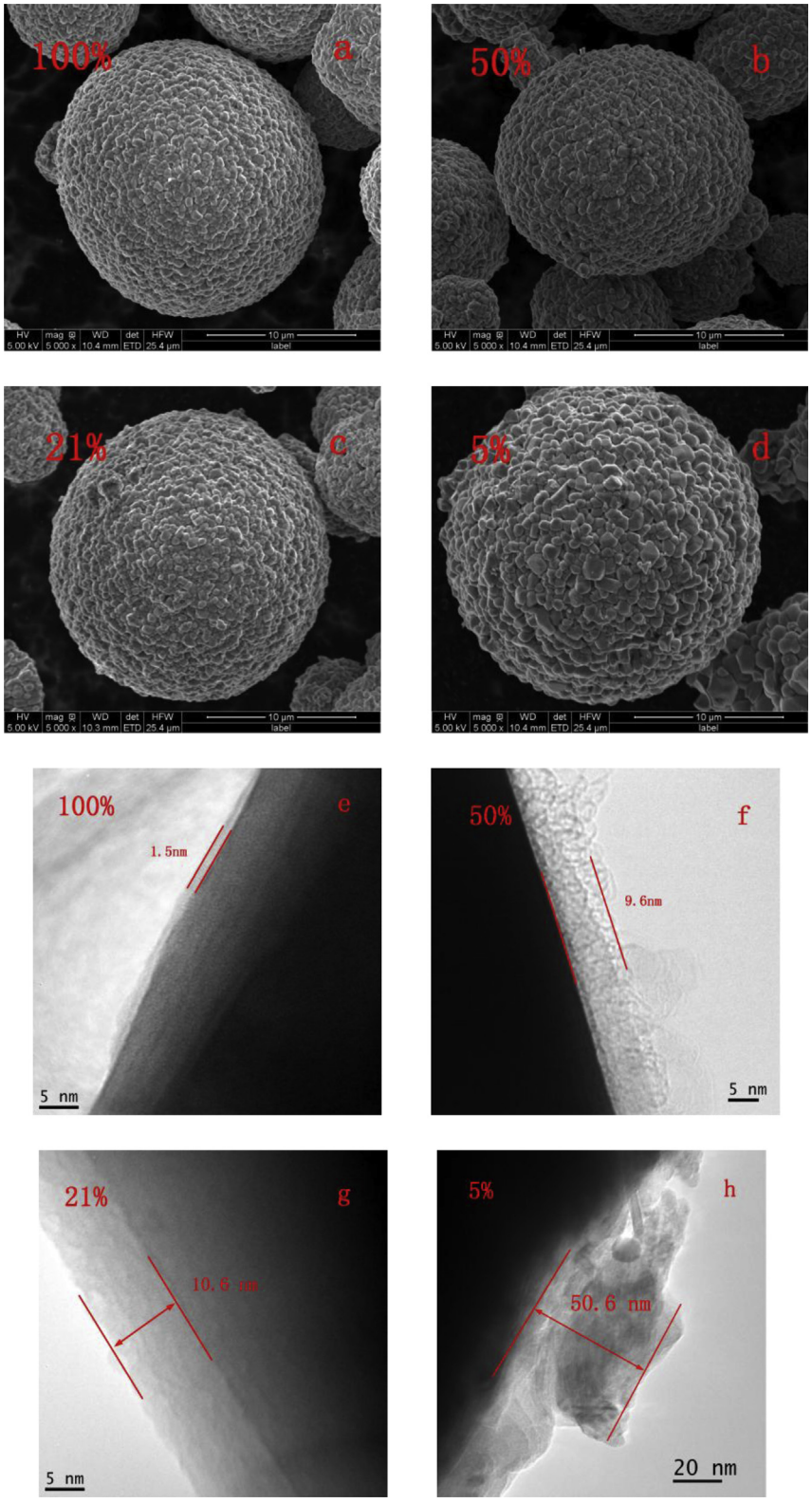

Fig. 3. Electron microscopy analysis of prepared $LiNi_{0.8}Co_{0.1}Mn_{0.1}O_2$ samples. a)–d), SEM images; e)-h) HRTEM images.

2.2. Electrochemistry

The slurry comprised of 80 wt% the prepared material, 10 wt% super P and 10 wt% polyvinylidene fluoride dissolved in *N*-methylpyrrolidone was coated on aluminum foil current collectors after stirring 4 h. The sheets were dried at 120 °C under vacuum, punched into φ16 mm disks. CR2032 coin cells were assembled with the prepared electrode as cathode, lithium foil as anode, Celgard 2550® as separator and 1 mol/L $LiPF_6$ in mixture solution of ethylene carbonate(EC)/diethyl carbonate(DEC)/ethyl methyl

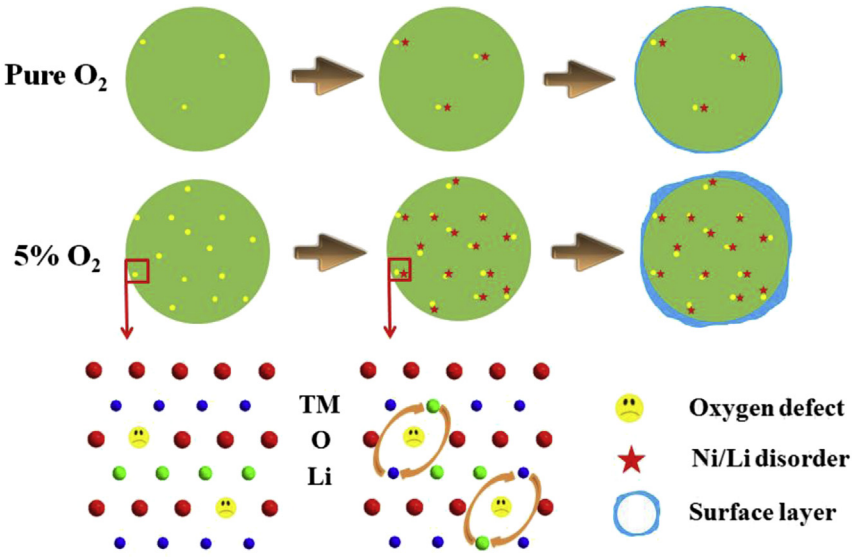

Scheme 1. Influence of oxygen defect on structural instabilities.

carbonate(EMC) as electrolyte. The assembly of the test cells was performed in Ar-filled M-Braun glove box, where H_2O and O_2 were controlled less than 1 ppm. The electrochemical measurements were performed on battery tester of Land 2001A (Wuhan, China) between 2.8 and 4.3 V *vs*. Li/Li^+ at 25 °C under various rates. In this work, 1C was named as 180 mAg^{-1}. The electrochemical impedance spectroscopy (EIS) of the coin cells were measured over the frequency range of 0.1 MHz to 0.1 Hz in a charge state of 4.3 V at CHI600D electrochemistry work station.

2.3. Characterization

The crystalline phase of prepared powders were characterized by X-ray diffraction with Bruker D8 advanced diffractometer using Cu$K\alpha$ ($\lambda = 1.5406$ Å) radiation (Bruker AXS, D8 Advance) between 10 and 135° by 0.02° step per second. The Rietveld refinements were carried out by using GSAS program via the EXPGUI interface. [27,28] The analysis of microscopy was performed with scanning electron microscopy (SEM, FEI, QUANTA 250 FEG) and transmission electron microscopy (TEM, JOEL 2100, 200 kV). Surface analysis was conducted with a PHI 3056 X-ray photoelectron spectrometer (XPS) which was excited by an Mg$K\alpha$ radiation at a constant power of 100 W (15 kV and 6.67 mA). The spectrum fitting was performed with CasaXPS software. Thermo-gravimetry (TG, Perkin–Elmer Pyris Diamond TG/DTA) was used to assess the oxygen non-stoichiometry in prepared sample with heat-cool rate 5 °C/min under the atmospheres of pure oxygen, O_2/N_2 (50: 50, 21: 79, 5: 95, v/v).

To improve the consistency, it should be noted that all samples were calcined in four same-model ovens at the same time, stored in the same desiccator and carried out all measurements within the same batch.

3. Result and discussion

The prepared materials are pure phase, which is attributed to *R*-3*m* group of hexagonal system, *iso*-structural to α-$NaFeO_2$, as shown in Fig. 1a. XRD patterns were further analyzed with GSAS, as shown in Fig. 1b, to compare the variations of structural parameters and the obtained results were briefed in Table 1. Ni/Li disorder ratio of the prepared samples is gradually lessened from 10.97% to 2.85% as the increase of oxygen partial pressures as shown in Table 1. On account of the difference between Ni and Li ions, the lattice parameter *c* is lowered when Ni/Li disorder goes seriously. The relationship between Ni/Li disorder and O_2 ratio in the sintering atmosphere is consistent with the previous proposed results. [29] Furthermore we also noticed that the occupancy of oxygen atom at 6c site in *R*-3*m* structure is gradually augmented as the increase of oxygen ratio.

Besides XRD refinements, the oxygen-keeping capability of the prepared materials was also qualitatively analyzed with thermo-gravimetry (TG) as desmostrated in Fig. 2. To eliminate the influence of the decomposed species from $LiNi_{0.8}Co_{0.1}Mn_{0.1}O_2$ that will be discussed in the latter part, the sample prepared under pure O_2 was used as the standard sample and checked its weight loss between room temperature to 850 °C under the investigated atmospheres. This test method is different from the regular way to measure the weight-gain of the synthesized samples under pure oxygen.

As shown in Fig. 2, the standard material shows the best oxygen-keeping capability under pure O_2, only lose 0.24 wt%. The weight loss becomes more obvious as the decrease of oxygen ratio. It loses 0.56 wt% and 1.01 wt% under the atmosphere containing 50% and 21% oxygen, respectively. The largest amount of weight-loss is observed under the atmosphere with 5% O_2, reaches to 2.14 wt%. According to our XRD and TG results, high-nickel cathodes are inevitably to lose oxygen atoms and generate oxygen defects, which amount are augmented as the decrease of oxygen proportion in sintering atmosphere. We also notice the weight gain for the samples tested under the atmosphere with 5% and 21% O_2 during cooling. It also indicates that the oxygen deficiency could be influenced by the calcination procedure.

The analysis of electron microscopy is shown in Fig. 3. The samples after sintering keep the similar spherical morphology of precursors, which are ~10 μm grains accumulated with 400–500 nm primary particles as revealed in Fig. 3a–d. The zooming-in observation with HRTEM (Fig. 3e–h) identifies a thin film formed on the surface of cathode particles. This unexpected layer is ~1.5 nm for the material prepared under pure oxygen (Fig. 3e), then gradually thickened to 9–10 nm as oxygen proportion was lowered to 50% and 21% (Fig. 3f and g), and finally augmented to more than 50 nm under the atmosphere with 5%

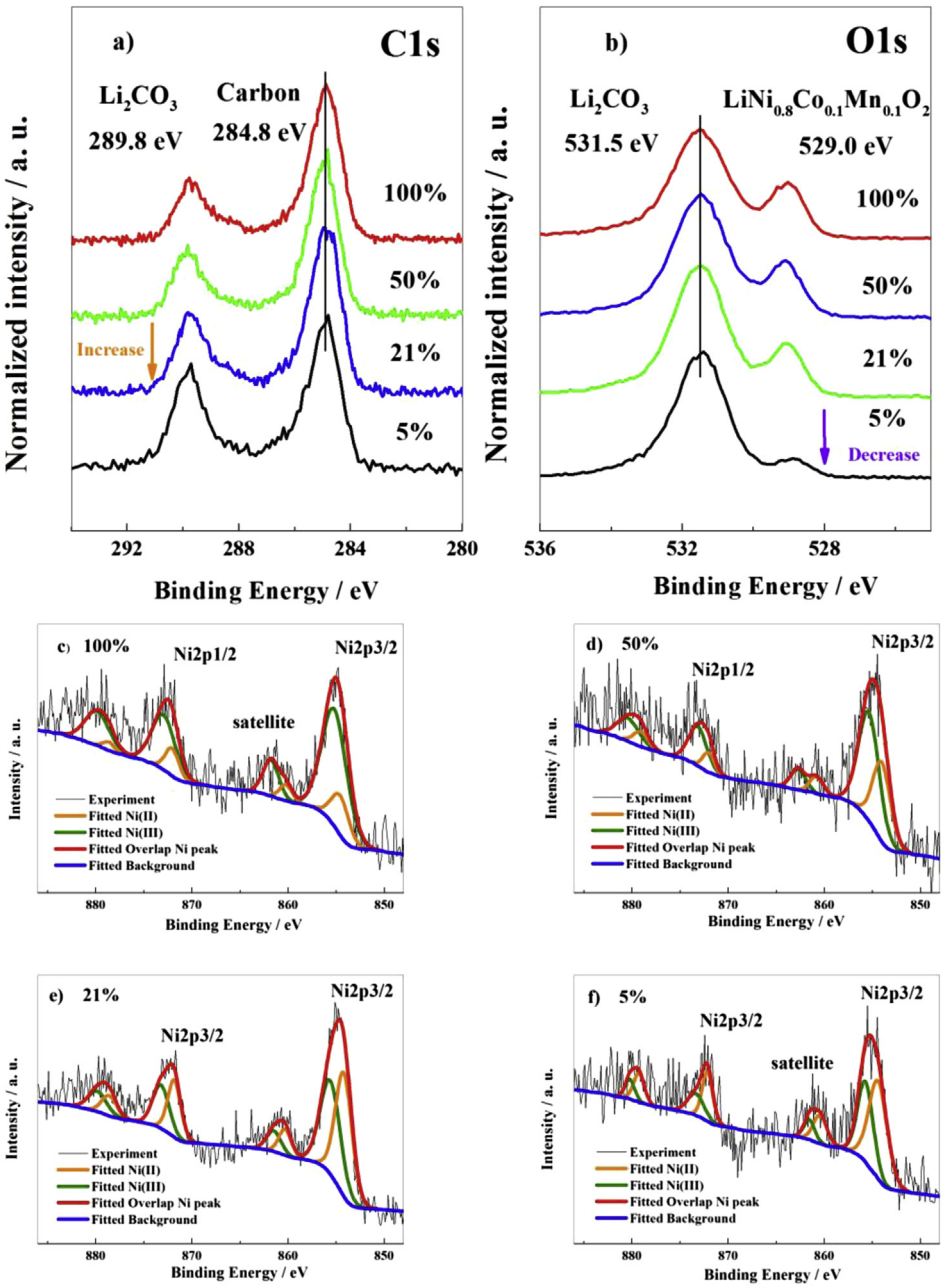

Fig. 4. XPS analysis of the prepared samples. a) C1s spectra; b) O1s spectra; c) – f) experiment and fitted of nickel 2p spectra.

Table 2
Ni 2p XPS fitted results.

Oxygen proportion	100%	50%	21%	5%
Ni^{2+}/at. %	25.8	37.7	51.3	60.1
Ni^{3+}/at. %	74.2	62.3	48.7	39.9

oxygen (Fig. 3h). It indicates that the rate of this surface decomposing reaction is accelerated at the low content of oxygen, namely the oxygen defects.

According to our results, the probable relation between oxygen non-stoichiometry and Ni/Li disorder & surface sensitivity is illustrated in Scheme 1. As oxygen releases from the lattice, Ni(III) ions should be reduced to Ni(II) simultaneously according to the principle of the electric neutrality. Then the local structure should be relaxed to reach a new equilibrium state. This relaxation should be similar to Li_2MnO_3's structural assignment, which is triggered by oxygen releasing during the first charge. [30] Since $LiNi_{1/3}Co_{1/3}Mn_{1/3}O_2$ and $LiNi_{0.4}Co_{0.2}Mn_{0.4}O_2$ don't suffer in Ni/Li disorder, the presence of Ni(II) is not the reason for this structural variation. Instead, local structural distortion caused by oxygen defects should be the driving force, which should lower the energy barrier of Ni(II) and Li(I) exchanging positions and enable the aforementioned structural relaxation. Obviously, the Ni/Li disorder is strengthened as the enhancement of oxygen deficiency.

The species accumulated on the particles should be the products of $LiNi_{0.8}Co_{0.1}Mn_{0.1}O_2$ decomposition. For all samples are stored in the same atmosphere and period, the variation of layer thickness is only related to the characteristics of materials' surface. [31] Similar to the oxygen deficiency in bulk, the sample synthesized under 5%

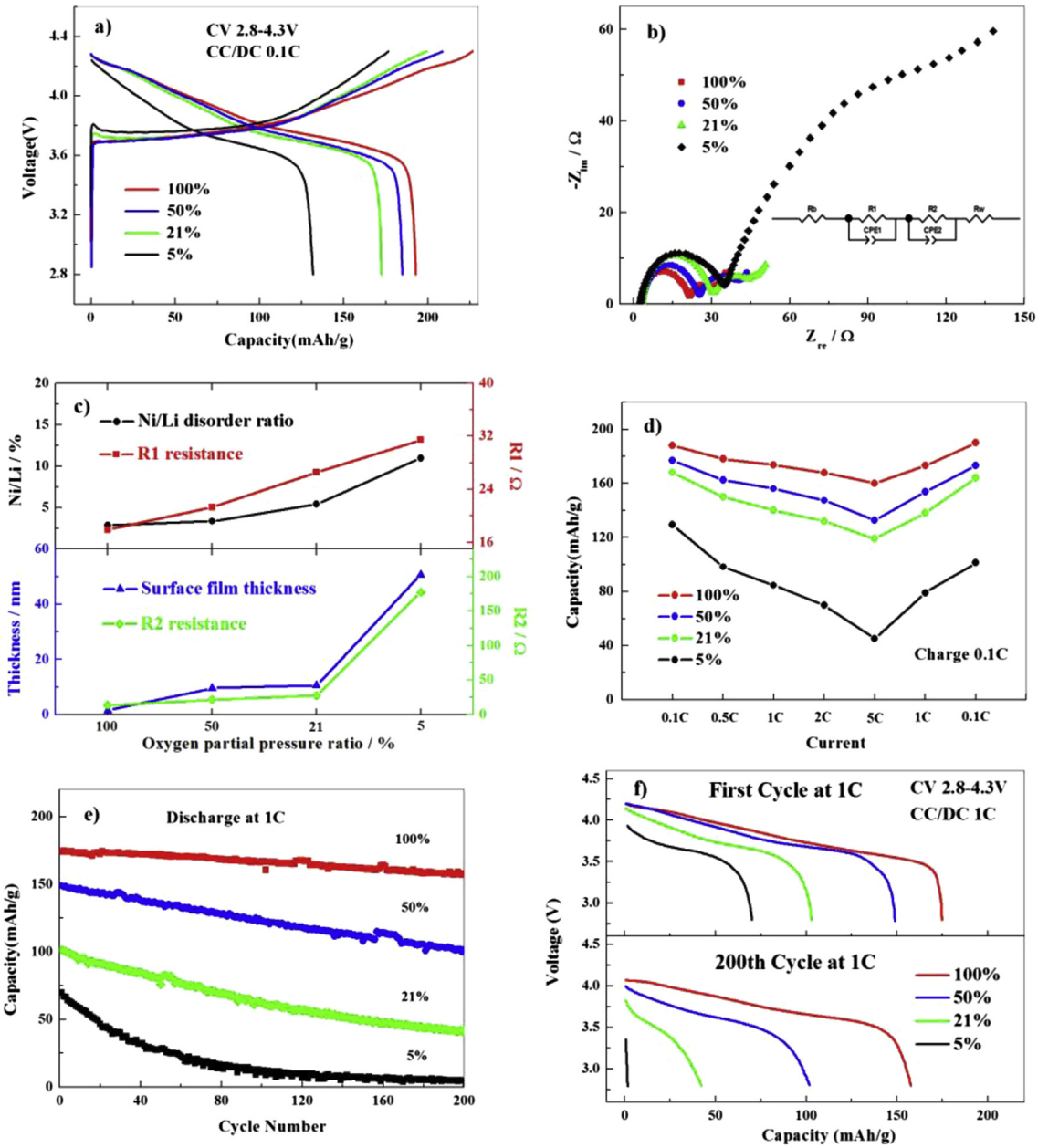

Fig. 5. Electrochemical properties of $LiNi_{0.8}Co_{0.1}Mn_{0.1}O_2$ cathode. a) initial capacity at 0.1C between 2.8 and 4.3 V *vs.* Li/Li^+; b) EIS spectra in a charge state of 4.3 V and corresponding equivalent circuit; c) the fitted R_1 and R_2 *vs.* oxygen defect ratio and surface thickness plot; d) rate capacity at 0.1, 0.5, 1, 2, 5C; e) cycling properties at 1C under 25 °C; d) charge and discharge curves of 1st and 200th cycle at 1C.

oxygen should keep the highest concentration of oxygen defects on its surface. Correspondingly, the largest amount of decomposing products is observed for this sample. Therefore the oxygen non-stoichiometry should accelerate the decomposing reaction during storage. According to our results, the strong catalytic capability of high Ni content cathode should be related to the generated oxygen defects, instead of the existence of Ni (II).

The prepared samples were investigated with X-ray photoelectron spectroscopy to analyze the components on their surface. Two types of chemical environments are identified for carbon and oxygen. As shown in Fig. 4a, besides the peak at 284.8 eV that is used as internal calibrator, a new carbon peak is identified at 289.8 eV, which could be attributed to Li_2CO_3. [32] O1s spectrum comprises of two peaks centered at 531.5 eV and 528.9 eV in Fig. 4b, which could be assigned to $LiNi_{0.8}Co_{0.1}Mn_{0.1}O_2$ and Li_2CO_3 respectively. After calibrating the peak intensities with the hypothesis that the samples contains the same amount of internal calibrator carbon, the intensities of C1s and O1s from Li_2CO_3 are monotonically weakened as the decrease of oxygen defects (as show in Fig. 4a and b). This trend is consistent with the thickness of surface layer observed with HRTEM results. Obviously, Li_2CO_3 is one of the key species composed of this auto-generated surface layer.

Chemical environment of nickel was also analyzed with XPS. As shown in Fig. 4c–f, both Ni(II) and Ni(III) co-exists on the sample's surface. The relative ratios of Ni(II) and Ni(III) were calculated by fitting nickel spectra and briefed in Table 2. The proportion of Ni(II) is around 25.8% for the material prepared under pure oxygen, indicating manganese and cobalt existed as a high oxidative

valence of 4+. The content of Ni(II) is quickly augmented to 37.7% and 51.3% for the samples synthesized under N_2+O_2 (50: 50, 79: 21), and even reached to 60.1% for the sample sintered under the atmosphere of 5% oxygen. The incremental of Ni(II) should correspond to another component decomposed from $LiNi_{0.8}Co_{0.1}Mn_{0.1}O_2$ and accumulated on the particle surface.

According to XPS results, the dominant species of decomposition on $LiNi_{0.8}Co_{0.1}Mn_{0.1}O_2$ surface are Li_2CO_3 and Ni(II), which are the same as that of $LiNi_{0.8}Co_{0.15}Al_{0.05}O_2$ [32–34]. Different from the previously proposed mechanism (Eq. (1)) on high-nickel cathode, the driving force for this reaction should be oxygen defects and the conjectural decomposing reaction should be modified to Eq. (2). It needs to be noted that $LiNiO_2$, instead of $LiNi_{0.8}Co_{0.1}Mn_{0.1}O_2$, is represented as cathode materials for convenience. Since CO_2 is involved into the reaction as the precursor, material decomposition should be taken place when encountered to air atmosphere. The oxygen defects could accelerate the decomposing reaction, probably through facilitating the absorption of humidity and/or carbon dioxide. Therefore the remedies to keep away from H_2O/CO_2-containing environment and to improve crystallographic entirety should be the effective way to suppress this unexpected surface decomposing reaction.

$$4LiNiO_2 + 2CO_2 \rightarrow 4NiO + 2Li_2CO_3 + O_2 \quad (1)$$

$$4LiNiO_{2-x} + 2CO_2 \rightarrow 4NiO + 2Li_2CO_3 + (1-2x)O_2 \quad (2)$$

Ni/Li disorder and surface layer play a detrimental effect on the electrochemical performance of high-nickel cathodes. Besides lowering the theoretical capacity, the nickel ions in lithium layer would block the transporting passage of Li^+ ions, and surface illustrative membrane lifts the energy barrier of the ion transportation. Therefore both instabilities could seriously aggravate the polarization and results in the poor kinetics.

The electrochemical performance of the investigated samples is compared in Fig. 5. The initial discharge capacity presents the obvious dependence on the extent of oxygen deficiency. As shown in Fig. 5a, the samples tested under 0.1C deliver discharge capacities as high as 131.1, 172.4, 184.8 and 192.9 mAh g^{-1} respectively, as the atmosphere contains 5, 21, 50 and 100% oxygen. Correspondingly, the variation among the discharge curves indicates the decrease of discharge capacity should be related to the augmented polarization. As revealed in Fig. 5a, the middle potential in discharge curves of pure oxygen synthesized sample is 52.7 mV higher than the 5% oxygen synthesized sample.

EIS was used to further analyze the variation of polarization in the electrochemical processes. As shown in Fig. 5b and c, the first semi-circle should be revealed the behavior of charge diffusion in bulk for R1 is almost linearly augmented as the increase of Ni/Li disorder. The semi-circle at low frequency should be corresponding to the step of charge's transportation through surface film for R2 is almost presents the same varying trend as surface-film thickness. It seems that the Ni/Li disorder and surface decomposition induced by oxygen defects could seriously deteriorate the kinetics of charge's transportation.

The rate capability is compared in Fig. 5d. The sample obtained under pure oxygen presents the best rate capability, attaining 173.7, 167.8, and 160.1 mAhg^{-1} at 1C, 2C and 5C. The materials prepared under 50% and 21% O_2 deliver a good rate capability, attaining 132.4 and 119.6 mAhg^{-1} at 5C, respectively. $LiNi_{0.8}Co_{0.1}Mn_{0.1}O_2$ calcined in 5% oxygen shows the worst kinetic behavior, only 45.3 mAhg^{-1} is obtained at 5C. This dependence on the oxygen proportion in sintering atmospheres could be attributed to the enhanced polarization from bulk and surface layer.

The cyclic stability is demonstrated in Fig. 5f. The sample prepared under pure O_2 behaves the best cyclic stability, attained 89.9% at 200th. As the decrease of oxygen ratio in sintering atmosphere, the samples present poor retention ratio, only 67.9%, 40.7% and 7.1% remained, respectively. As shown in Fig. 5g, the samples with more oxygen defects exhibit much higher polarization. This deterioration should be partially related with the decomposition of Li_2CO_3 in surface layer, which will be discussed in another works.

4. Conclusion

The influence of oxygen non-stoichiometry on the structure and electrochemical performance of $LiNi_{0.8}Co_{0.1}Mn_{0.1}O_2$ has been investigated in this work. The oxygen defects should trigger Ni/Li exchanging positions in the bulk, and accelerate the decomposition on surface. The increase of oxygen deficiency significantly strengthened the aforementioned instabilities, which seriously deteriorate the electrochemical performance due to the heavily aggravated polarization. Therefore, the improvement on oxygen-keeping capability should play a positive role on the behavior of high-nickel cathodes.

Acknowledgments

This work was supported by 863 project (Grant No. 2013AA050906), Zhejiang Key Innovation Team (Grant No. 2013PT16), the "Strategic Priority Research Program" of the Chinese Academy of Sciences (Grant No. XDA09010403), and Hundred Talents Program of the Chinese Academy of Sciences.

References

[1] M. Armand, J.-M. Tarascon, Nature 451 (2008) 652.
[2] D.D. MacNeil, Z. Lu, J.R. Dahn, J. Electrochem. Soc. 149 (2002) A1332–A1336.
[3] N. Yahuuchi, T. Ohzuku, J. Power Sources 119–121 (2003) 171–174.
[4] Z. Wang, Y. Sun, L. Chen, X. Huang, J. Electrochem. Soc. 151 (2004) A914–A921.
[5] Y. Koyama, Y. Makimura, I. Tanaka, H. Adachi, T. Ohzuku, J. Electrochem. Soc. 151 (2004) A1499–A1506.
[6] P. He, H. Yu, D. Li, H. Zhou, J. Mater. Chem. 22 (2012) 3680–3695.
[7] Y. Sun, C. Ouyang, Z. Wang, Z. Wang, X. Huang, L. Chen, J. Electrochem. Soc. 151 (2004) A504–A508.
[8] Y.K. Sun, S.T. Myung, B.C. Park, J. Prakash, I. Belharouak, K. Amine, Nat. Mater. 8 (2009) 320–324.
[9] M. Jo, M. Noh, P. Oh, Y. Kim, J. Cho, Adv. Energy Mater. 4 (2014), 1301583.
[10] K. Du, C. Hua, C. Tan, Z. Peng, Y. Cao, G. Hu, J. Power Sources 263 (2014) 203–208.
[11] H. Konishi, M. Yoshikawa, T. Hirano, J. Power Sources 244 (2014) 23–28.
[12] K.S. Lee, S.T. Myung, K. Amine, H. Yashiro, Y.K. Sun, J. Electrochem. Soc. 154 (2007) A971–A977.
[13] S.K. Martha, H. Sclar, Z.S. Framowitz, D. Kovacheva, N. Saliyski, Y. Gofer, P. Sharon, E. Golik, B. Markovsky, D. Aurbach, J. Power Sources 189 (2009) 248–255.
[14] G.Y. Kim, J.R. Dahn, J. Electrochem. Soc. 160 (2013) A1108–A1111.
[15] Z. Lu, D.D. MacNeil, J.R. Dahn, Solid State Lett. 4 (2001) A200–A203.
[16] H. Liu, Z. Zhang, Z. Gong, Y. Yang, Solid State Ionics 166 (2004) 317–325.
[17] K. Kang, G. Ceder, Phys. Rev. B 74 (2006) 094105–094111.
[18] Y. Koyama, H. Arai, I. Tanaka, Y. Uchimoto, Z. Ogumi, J. Power Sources 244 (2014) 592–596.
[19] H. Yu, Y. Qian, M. Otani, D. Tang, S. Guo, Y. Zhu, H. Zhou, Energy Environ. Sci. 7 (2014) 1068–1078.
[20] D.D. MacNeil, Z. Lu, J.R. Dahn, J. Electrochem. Soc. 149 (2002) A1332–A1336.
[21] W.A. Harrison, Phys. Rev. B 73 (2006) 212103.
[22] Y. Koyama, H. Arai, I. Tanaka, Y. Uchimoto, Z. Ogumi, Chem. Mater. 24 (2012) 3886–3894.
[23] Y. Koyama, H. Ariai, I. Tanka, Y. Uchimoto, Z. Ogumi, J. Mater. Chem. A 2 (2014) 11235–11245.
[24] C.L. Freeman, J.A. Dawson, H.R. Chen, L. Ben, J.H. Harding, F.D. Morrison, D.C. Sinclair, A.R. West, Adv. Funct. Mater. 23 (2013) 3925–3928.
[25] D.A. Tompsett, S.C. Parker, M.S. Islam, J. Am. Chem. Soc. 136 (2014) 1418–1426.
[26] G. Campi, A. Ricci, N. Poccia, A. Bianconi, J. Supercond. Nov. Magn. 27 (2014) 987–990.
[27] B.H. Toby, J. Appl. Crystallogr. 34 (2001) 210–213.
[28] A.C. Larson, R.B. Von Dreele, Los Alamos Nat. Lab. Rep. (2004), 86–748.

[29] M. Sobri Idris, A.R. West, J. Electrochem. Soc. 159 (2012) A396–A401.
[30] S. Hy, F. Felix, J. Rick, W. Su, B.J. Hwang, J. Am. Chem. Soc. 136 (2014) 999–1007.
[31] D.H. Cho, C.H. Jo, W. Cho, Y.J. Kim, H. Yashiro, Y.K. Sun, S.T. Myung, J. Electrochem. Soc. 161 (2014) A920–A926.
[32] H. Liu, Y. Yang, J. Zhang, J. Power Sources 162 (2006) 644–650.
[33] H. Liu, Y. Yang, J. Zhang, J. Power Source 173 (2007) 556–561.
[34] K. Shizuka, C. Hiyohara, K. Shima, J. Power Sources 166 (2007) 233–238.